Supplement of Atmos. Chem. Phys., 19, 2845–2860, 2019
https://doi.org/10.5194/acp-19-2845-2019-supplement

Atmospheric Chemistry and Physics
Open Access
EGU

Supplement of

Characterization of ozone production in San Antonio, Texas, using measurements of total peroxy radicals

Daniel C. Anderson et al.

Correspondence to: Daniel C. Anderson (dca54@drexel.edu)

Supplementary Information

S1. ECHAMP Inlet Description

A schematic of the ECHAMP inlet used during SAFS is shown in Fig. S1. As described in the main text, the inlet was mounted approximately 15 m above ground level. Solenoid valves were located inside the AML, and gases were transported to the inlet through 22.8 m of 3.2 mm (1/8") OD FEP tubing for NO and copper tubing for N_2 and C_2H_6. At any given point in time, one reaction chamber was in amplification mode (C_2H_6 added upstream, N_2 added downstream) and the other was in background mode (N_2 added upstream, and C_2H_6 added downstream). This inlet differs from that described in Wood et al. (2017) in that a RO_X calibration system based on water vapor photolysis (described in Sect. S2.1) was permanently connected to the inlet, so that calibrations could be performed without disturbing sampling from the other instruments. During calibrations, zero air was delivered by 22.8 m of 9.5 mm (3/8") OD FEP tubing to a 12.7 mm (0.5") OD quartz tube inside the inlet box

S2. XO_2 Calibrations

Total peroxy radicals were calibrated using two methods: photolysis of H_2O followed by reaction with either H_2 or C_2H_6 and photolysis of CH_3I. We describe both methods here.

S2.1. H_2O calibration

Calibration of XO_2 was performed via water vapor photolysis at 184.9 nm from a mercury lamp, which produces an equimolar mixture of OH and HO_2, according to Reaction (RS1) (Schultz et al., 1995;Lanzendorf et al., 1997). The OH was then reacted with H_2 (g) which was added to the zero air flow upstream of the UV illumination to quantitatively convert OH into HO_2 (Reaction RS2).

$$H_2O + h\upsilon + O_2 \rightarrow OH + HO_2 \quad \text{(RS1)}$$
$$OH + H_2 + O_2 \rightarrow HO_2 + H_2O \quad \text{(RS2)}$$

Total XO2 can then be calculated from Eq. (S1), where brackets denote concentration, σ and φ are the absorption cross sections and photolysis quantum yields at 185 nm for the indicated species, respectively. For σ_{H2O} we use 7.1×10^{-20} cm^2 molecule^{-1} (Cantrell et al., 1997). The effective O_2 absorption cross section depends on both the UV lamp operating conditions and the O_2 column density

and therefore must be characterized for each lamp (Lanzendorf et al., 1997;Creasey et al., 2000). The Hg lamp used in this study was characterized at the University of Indiana courtesy of Phil Stevens and found to have an effective cross section of 1.3×10^{-20} cm^2 molecule^{-1} at an O_2 column density of 5×10^{18} molecules cm^{-3}, within the range of values seen in other studies (Lanzendorf et al., 1997;Creasey et al., 2000). Quantification of the ozone formed by photolysis of O_2 at the same wavelength (184.9 nm) serves as the "chemical actinometer" (Schultz et al., 1995).

$$[HO_2] + [RO_2] = \frac{[O_3][H_2O]\sigma_{H2O}\phi_{H2O}}{[O_2]\sigma_{O2}\phi_{O2}} \quad \text{(S1)}$$

The typical calibration procedure is as follows:

1. 8 to 10 LPM of dry zero air (ZA) flow sequentially through 22.8 m of 9.5 mm (3/8") OD FEP tubing, an 18 cm long 12.7 mm (0.5") quartz tube in the ECHAMP inlet box, and into the sampling manifold (see Fig. S1). Both reaction chambers are operated in background mode, with NO and N_2 added upstream of the reaction chambers and ethane added downstream. The NO_2 concentration measured by the CAPS sensors for this step is solely from impurities in the NO flow and NO_2 formed by the termolecular reaction between NO and O_2.
2. A mercury lamp (Jelight 78-2046-2) mounted onto the outside of the quartz tube is then turned on, providing UV radiation at 184.9 nm and resulting in the production of O_3 in the ZA flow but no HO_X given the absence of $H_2O_{(g)}$. A nitrogen purge was placed between the lamp and the quartz tubing to prevent ozone formation outside of the sampling system. Only a small portion of the quartz tubing (~1 cm) is exposed to the lamp to control the eventual HO_X and O_3 concentrations. The ozone reacts with the excess NO to produce NO_2. The ozone concentration for Eq. (S1) is thus given by the difference in measured [NO_2] between steps 1 and 2 of the calibration, with a 10% correction applied to account for the dilution by the added flows of NO, N_2, and C_2H_6. Typical O_3 concentrations for calibration were between 0.5 and 2 ppbv, which is

easily measured with the CAPS sensors given their typical NO_2 precision of 20 pptv with 10-second averaging.

3. A portion of the ZA is then sent through a bubbler system with distilled water to humidify the ZA flow. The H_2O concentration for Eq. (S1) is calculated using the RH and temperature reading form the Vaisala probe and the ambient pressure.
4. H_2 gas was then added to the mixture at a flow rate of 30 sccm. ECHAMP was then operated in normal sampling mode, with the two reaction chambers alternating between amplification and background modes every 60 s.

The amplification factor, F, is then determined from the ratio of the observed change in NO_2 signal during step 4 (amplification mode) to the XO_2 concentration calculated from Eq. (S1).

S2.2. CH_3I calibration

The CH_3I photolysis method, similar to the acetone photolysis method described in Wood and Charest (2014) except that methyl iodide is used in place of acetone, produces methyl peroxy radicals (CH_3O_2) by the UV photolysis of CH_3I(g):

$$CH_3I + 254\ nm \rightarrow CH_3 + I \quad \text{(RS3)}$$
$$CH_3 + O_2 + M \rightarrow CH_3O_2 + M \quad \text{(RS4)}$$

In both cases, the peroxy radical concentration is quantified simply by the increase in NO_2 following reaction of the peroxy radicals with excess NO. The concentration quantification does not rely on spectroscopic parameters or direct actinometry of the UV source, but instead on the accuracy of the NO_2 measurements by the CAPS, which we trace to the absorption cross section of O_3 at 254 nm, and the relative rate constants for reactions.

The source of CH_3I is a permeation tube (KynTek, 1.8 µg/min permeation rate at 35° C), held at 55° C. We flow approximately 100 sccm of N_2 through the permeation tube and dilute this into a larger flow of 8 LPM of either dry or humidified ultra zero air, resulting in an estimated CH_3I mixing ratio of 80 ppbv based on the manufacturer-stated permeation rate and assuming the permeation rate is twice as high

at 55° C. This diluted CH_3I then enters a Pyrex photolysis chamber (volume 50 cm^3) into which an "O_3-free" mercury lamp is inserted (Jelight model 81-3306-2, all 185 nm radiation blocked).

When these CH_3O_2 radicals enter the reaction chamber that is in "background" mode, i.e., with the C_2H_6 added downstream of the NO addition, allowing time for all sampled ROx to be converted to HONO, the following reactions occur:

$$CH_3O_2 + NO \rightarrow CH_3O + NO_2 \quad \text{(RS5)}$$
$$CH_3O + O_2 \rightarrow HCHO + HO_2 \quad \text{(RS6)}$$
$$CH_3O + NO + M \rightarrow CH_3ONO + M \quad \text{(RS7)}$$
$$HO_2 + NO \rightarrow OH + NO_2 \quad \text{(RS8)}$$

Thus by modulating the CH_3O_2 source and observing the change in NO_2, the concentration of CH_3O_2 can be calculated based on the overall stoichiometry of Reactions (RS5) through (RS8). Modulating the NO flow on and off instead of the CH_3O_2 source would be inferior because it would also remove the NO_2 already present in the NO flow due to impurities and the termolecular reaction between NO and O_2. The CH_3O_2 flow can be modulated in three ways: 1. Periodically diverting the CH_3I flow from the perm tube away from the air dilution flow (but with the zero air still illuminated by the UV lamp), 2. Turning the UV source on and off, or 3. Periodically having the diluted CH_3I + zero air flow bypass the UV chamber and proceed to the ECHAMP inlet.

Method 1 is similar to the acetone photolysis method described by Wood and Charest (2014) with the weakness that it will also remove any interfering species present in the permeation tube output that absorb blue light, e.g., I_2 or I_3^- compounds. The advantage of methods 2 and 3 are that any blue-absorbing species present in the gas mixture will always be present and thus not present an interference. This is important when using the CAPS monitor to quantify NO_2, since it measures the total cell absorption at 450 nm (FWHM 10 nm) and thus is not completely spectroscopically selective to NO_2. Method 2 suffers from the time required for the Hg lamp to warm-up. Method 3 is thus our primary method, though we periodically use methods 1 and 2 as a check. A schematic of the calibration setup is shown in Fig. S6.

There are two main parts to the calibration procedure:

1. CH_3I flows through the UV chamber, producing CH_3O_2 radicals, and the two channels of ECHAMP are operated in its standard operation mode, each channel alternating between amplification mode and background mode.
2. Both channels are kept in background mode, and the CH_3O_2 source is modulated as described above by periodically having the diluted CH_3I flow bypass the photolysis chamber.

The amplification factor is given by Eq. (S2):

$$F = \Delta NO_2(\text{step1}) / [CH_3O_2] \quad \text{(S2)}$$

ΔNO_2(step1) is the difference in $[NO_2]$ observed by ECHAMP during step 1 of the calibration procedure and $[CH_3O_2]$ is determined by the following equation:

$$[CH_3O_2] = \Delta NO_2(\text{step2}) / (1.86 \times 0.92) \quad \text{(S3)}$$

ΔNO_2(step2) is the change in $[NO_2]$ observed when the CH_3O_2 source is modulated during step 2. The factor of 1.86 accounts for the portion of the CH_3O_2 radicals that form CH_3ONO upon reaction with excess NO rather than two NO_2 molecules. This is calculated by Eq. (S4):

$$FF = 2\left\{\frac{k_{RS6}[O_2]}{k_{RS6}[O_2]+k_{RS7}[NO]}\right\} \quad \text{(S4)}$$

Where k_{RS6} (1.9×10^{-15} cm^3 $molecule^{-1}$ s^{-1}) and k_{RS7} (3.3×10^{-11} cm^3 $molecule^{-1}$ s^{-1}) are the rate constants for Reactions (RS6) and (RS7), respectively (Atkinson et al., 2006). The factor of 0.92 in Eq. (S2) accounts for the dilution of the gas by the added N_2, C_2H_6/N_2, and NO/N_2.

In contrast to the H_2O photolysis method, this CH_3I method is an "internal" calibration, i.e. the concentration determined is the amount that entered the reaction chamber - it does not account for losses of radicals in the sampling system. Separate wall loss measurements have demonstrated that losses of CH_3O_2 in our sampling inlet are negligible (less than 1%) and losses of HO_2 less than 3%. Sampling losses of CH_3O_2 and other peroxy radicals, especially HO_2, will be described in more detail in a future publication (Anderson et al, in preparation).

An example time series of CH_3I calibration data is shown in Fig. S7 from 31 May 2017. From 10:30 to 10:34 ECHAMP was operating in regular sampling mode (alternating amplification-background mode), sampling CH_3O_2 radicals from the CH_3I photolysis system at 23% RH, with a modulated NO_2 signal of 4.14 ppbv. From 10:34 to 10:40, the diluted CH_3I periodically bypassed the UV chamber, producing a modulated NO_2 signal of 0.37 ppbv. This results in an amplification factor of 19.1. During field calibrations we typically measure multiple single-point calibrations over a range of RH values. To confirm instrument linearity we occasionally execute multi-point calibrations over a range of concentrations at a single RH value. The uncertainty of this calibration method depends on the short-term precision and baseline drift of the CAPS monitors, the CAPS NO_2 calibration, the uncertainty in the NO and O_2 mixing ratios, and the rate constants for RS5, RS6, and RS7. For the calibration concentrations used during SAFS, the 2 sigma uncertainty of this method was 20%.

We have also investigated potential interferences due to I_2 formation. I_2 can also be formed following photolysis of CH_3I through the following mechanisms as described by Clemitshaw et al (1997):

$$I + I + M \rightarrow I_2 + M \quad \text{(RS9)}$$
$$I + NO + M \rightarrow INO + M \quad \text{(RS10)}$$
$$INO + INO \rightarrow I_2 + 2NO \quad \text{(RS11)}$$
$$CH_3O_2 + I + M \leftrightarrow CH_3O_2I + M \quad \text{(RS12)}$$
$$CH_3O_2I + I \rightarrow CH_3O_2 + I_2 \quad \text{(RS13)}$$

The maximum amount of I_2 that could be formed, based on Reactions (RS9), (RS11), and (RS13), is equal to $[CH_3O_2]/2$. At this amount, I_2 would be an interference as it absorbs blue light and would be detected as NO_2 by the CAPS sensor (I_2 absorption cross section at 450 nm is ~75% that of NO_2).

To determine experimentally whether there is any observable interference from I_2 formation, we determined the CH_3O_2 concentration as described in step 2 of the calibration procedure above. Then, we turned off the NO flow, effectively stopping amplification. Leaving the lamp on, we then periodically switched between flowing the CH_3I through the photolysis chamber and then bypassing photolysis. The difference in observed signal between these two settings would therefore stem from absorption of blue light from I_2. For a flow rate that produced 100 pptv of CH_3O_2, concentrations typically used for calibrating, the I_2 signal, if any, was indistinguishable from the instrument noise, suggesting that at this

concentration, there is negligible interference from I_2 in our calibration. For a flow rate that produced a CH_3O_2 concentration of 450 pptv, significantly larger than what is used for calibrations, the CAPS produced an "equivalent" NO_2 signal of ~100 pptv, which would lead to an overestimate in the CH_3O_2 concentration of 22%.

A simple computer numerical integration, using the above described reactions, was also used to calculate the variation in INO, I_2, and CH_3O_2I with time. Literature values were used for all rate constants except for reactions S12 and S13, for which literature values could not be found. Four simulations were conducted. In the first two, the rate constant for Reaction (RS12) (forward) was estimated as 1×10^{-11} cm^3 $molecules^{-1}$ s^{-1}, and the rate constant for the reverse (RS12) reaction, k was assumed to be 0. The initial concentrations of I and CH_3O_2 were 100 pptv in the first simulation and 1000 pptv in the second. In the third and fourth simulations, these initial concentrations were kept the same, while the reaction rates for S12 was increased to 1×10^{-10} cm^3 $molecules^{-1}$ s^{-1}. The simulations are summarized in Table S1. Table S2 shows the reaction rate constants for each reaction used in the simulation.

Each simulation showed that I_2 formation was negligible for the conditions used in calibration. In the presence of 1 ppmv NO, the simulations indicated that more than 99.9% of the I is rapidly converted to INO, leaving the INO self-reaction (Reaction RS14) as the only viable route to I_2 formation. The rate constant for this reaction is 1.3×10^{-14} cm^3 $molecules^{-1}$ s^{-1} (Atkinson et al., 2007) – 30 times slower than the effective 2nd-order rate constant for the direct recombination of atomic I (Reaction RS9). In addition, the simulation was repeated including the reaction of I with INO to form I_2 and NO, with no significant change to the results. We conclude that I_2 formation is negligible under the conditions of our calibrations, in agreement with our laboratory tests.

S2.3. Calibration Comparison

Figure S8 compares the CH_3I (blue circles) and H_2O photolysis (red, filled triangles) calibration methods from the SAFS campaign. Both methods agree within uncertainty. Variability in the F values likely results from variations in mercury lamp intensity, which during the campaign was only measured

when the ozone mixing ratio was quantified (via the change in [NO_2]) when the lamp was turned off. We use the CH_3I derived curve in this analysis because H_2O photolysis calibrations were all conducted at RH less than ~20%. Because increasing the RH also increases the HO_2 concentration in the H_2O photolysis calibration method, the UV lamp output must be attenuated to prevent super-ambient radical concentrations. During SAFS, a remote method of light attenuation was unavailable, and because the instrument inlet box was inaccessible without interrupting sampling for other instruments, we could not alter the H_2O photolysis setup. For RH greater than 20%, it was found that the resultant HO_2 concentration was unreasonably high (sometimes exceeding 1 ppbv), and we therefore limit results to below this value. To demonstrate that the H_2O photolysis calibration method is applicable over a wider range of RH, we show results from a subsequent field deployment in Bloomington, IN during July 2017 (Fig. S8, red, open triangles). While we would expect differences in the calibration results because the instrument configuration was different for this later deployment, the overall relationship between F and RH is similar at higher RH values.

S3. Isoprene

No isoprene standard was available during SAFS for online calibration of the GC-MS observations, so an isoprene sensitivity was not determined during the campaign. Approximately 6-months after SAFS, a calibration of the same instrument was conducted during a second campaign using a multi-component mixture, including isoprene and 6 other hydrocarbons (iso-pentane, *n*-pentane, *n*-hexane, methylcyclopentane, cyclohexane, and benzene) measured during SAFS. To determine a sensitivity for isoprene for SAFS, the sensitivities for the six hydrocarbons during SAFS was compared to that for the second campaign, in which the GC setup differed in both sample trap temperature and detector micro channel plate voltage from the SAFS configuration. The mean ratio of sensitivities from SAFS to the second campaign for the six overlapping hydrocarbons was 0.34 ± 0.10 (1σ), while the slope of a regression line of the SAFS sensitivities to the second campaign sensitivities was 0.38. The isoprene sensitivity for SAFS was then determined by dividing the sensitivity to isoprene at the second campaign

by the average of these two values (0.36). The total uncertainty (1σ) in the isoprene observations is estimated as 31%, with the sensitivity uncertainty dominating.

While there was an in-field calibration for the PTR derived isoprene, it was determined that the isoprene concentration in this older calibration tank was most likely lower than the stated value, biasing the PTR results. There were overlapping observations of the PTR and GC derived isoprene values from the start of the campaign to 19 May, after which the GC trap was damaged. So that we have calibrated isoprene observations for the duration of the campaign, we have scaled the PTR derived isoprene to GC values for this overlapping period. The 1-minute averaged PTR data were averaged to the GC sampling time, and a linear least squares regression was used to determine the relationship. This resulted in a fit with an r^2 of 0.91 and a relationship between the two instruments as follows: $[C_5H_8]_{GC} = 0.787[C_5H_8]_{PTR} - 0.15$ (Fig. S9). The normalized mean bias for this relationship was 7%.

To evaluate the scaled PTR isoprene, we compare these values to isoprene measurements made hourly by a GC at the Floresville TCEQ site. The scaled PTR isoprene was averaged to the TCEQ sampling frequency and regressed against the TCEQ isoprene. This yielded a slope of 0.93 with an r^2 of 0.88. There was an offset of 0.10 ppbv between the two data sets with the TCEQ isoprene higher. The excellent agreement between the scaled PTR isoprene and the TCEQ isoprene further validates the isoprene results presented here.

S4. Model Description

To calculate the L_N/Q parameter from Sect. 3.2 of the main text, we modeled the photochemistry with the Framework for 0-D Atmospheric Modeling (F0AM) version 3.1 box model (Wolfe et al., 2016). The model was run with a subset of the Master Chemical Mechanism (Jenkin et al., 2003;Saunders et al., 2003) version 3.3.1 (MCMv331) (Jenkin et al., 2015). F0AM was constrained with observations taken during SAFS of temperature, pressure, water vapor, O_3, NO_2, CO, CH_4, HCHO, methanol, acetone, acetaldehyde, isoprene, propane, ethane, ethyne, monoterpenes, toluene, *n*-pentane, *n*-hexane, *n*-heptane, *n*-octane, xylenes, ethyl benzene, 1,2,4-trimethylbenzene, benzene, and cyclohexane. Because there were

no speciated observations, all monoterpenes were assumed to be α-pinene. Likewise, observations of total *m*- and *p*-xylene were assumed to be a 50% mixture. Observational constraints were averaged over the 2-minute ECHAMP sampling interval, and only intervals with simultaneous observations of XO_2, CO, O_3, NO, water vapor, isoprene, and HCHO were used. Data from the GC, which had a sampling frequency lower than that of ECHAMP, were linearly interpolated to the ECHAMP sampling time. The modeled intervals were further restricted to sampling at a solar zenith angle (SZA) less than 80°. Missing data were linearly interpolated in time. For photolysis reactions, the model was constrained to observations of J_{NO2}. Other photolysis rates were determined from a lookup table of values calculated by the TUV model as described in Wolfe et al. (2016). These values were then scaled to the observed JNO_2. The model was run forward in time with a model time-step of 1 hour, with all constrained concentrations and meteorology held constant but photolysis frequencies varying with time of day. The diurnal cycle was repeated for 4 days for each set of observations, which was found sufficient to bring XO_2 into steady state.

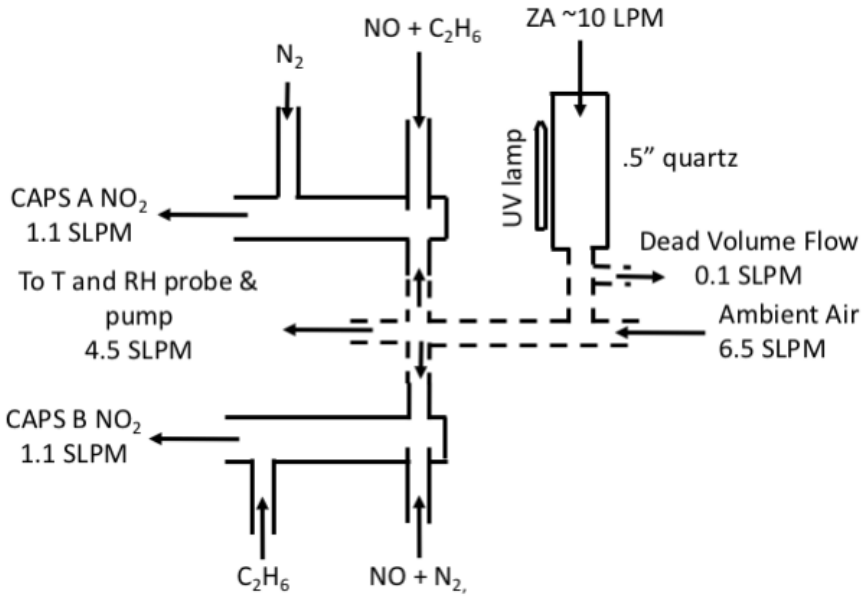

Figure S1: A schematic of the ECHAMP inlet used during SAFS. Dashed lines represent glass coated in halocarbon wax. The ZA flow is only used during H_2O based calibrations. As drawn, the upper reaction chamber (Chamber A) is in amplification mode (C_2H_6 added upstream, N_2 added downstream) and the lower reaction chamber (Chamber B) is in background mode. Every minute, the C_2H_6 and N_2 flows are switched so that the reaction chamber that was in amplification mode is then in background mode and vice versa. The upstream and downstream additions are ~15.2 cm apart, and the reaction chamber continues for another 66 cm before entering a filter. C_2H_6 was a 42.2% in N_2 mixture and was flowed at 35 sccm; NO was a 39.2 ppmv in N_2 mixture and was flowed at 25 sccm. The N_2 flow rate was 35 sccm.

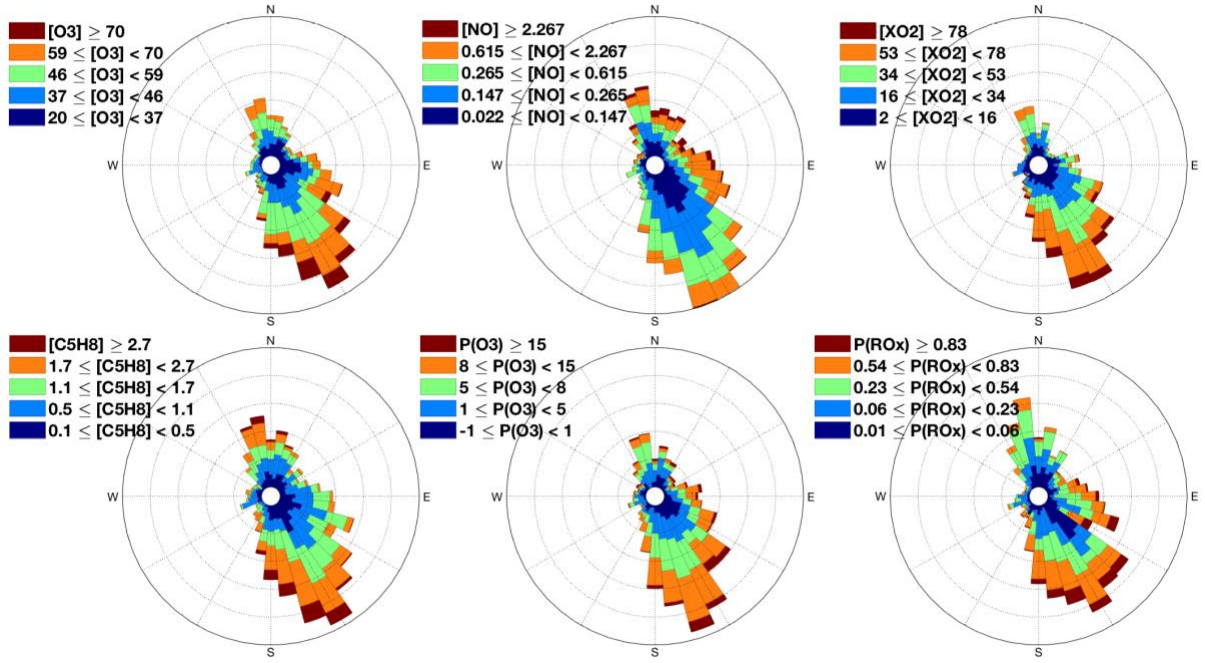

Figure S2: Wind roses showing the variation in O_3 (a), NO (b), XO_2 (c), isoprene (d), $P(O_3)$ (e), and $P(RO_X)$ (f) with direction for all observations at the UTSA site. Observations are separated into their 5th, 25th, 50th, 75th, and 95th percentiles for each species.

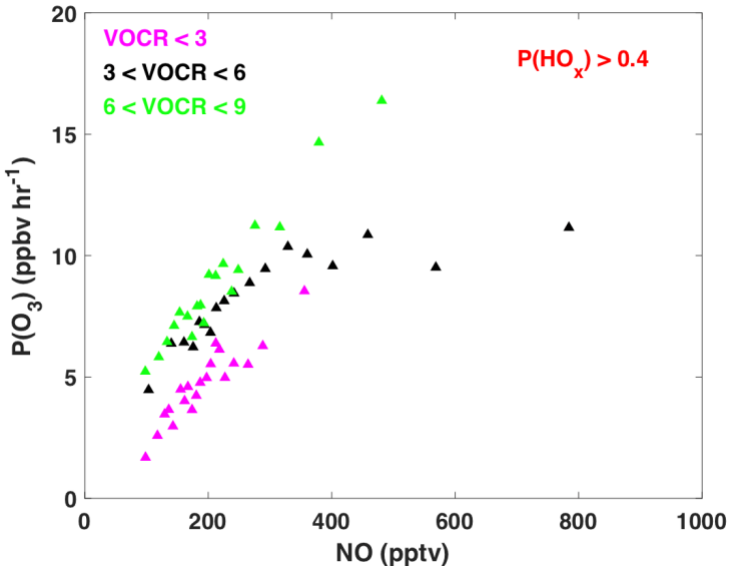

Figure S3: Same as Figure 6c except for $P(HO_X)$ > 0.4 pptv/s. The subset of observations with $P(RO_X)$ > 0.4 pptv s^{-1} are separated into three categories: low VOC reactivity (VOCR < 3 s^{-1}; magenta), medium VOC reactivity (3 < VOCR < 6 s^{-1}; black), and high VOC reactivity (6 < VOCR < 9 s^{-1}; green). As in Figure 6b, data are separated into NO bins with equal numbers of observations in each bin.

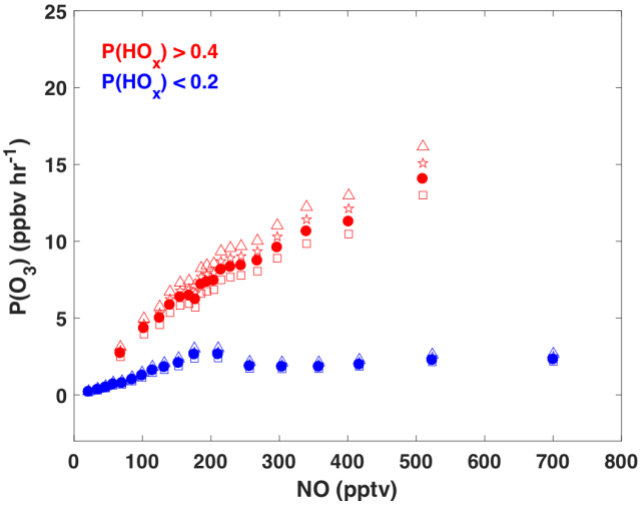

Figure S4: The variation of $P(O_3)$ with NO for all daytime observations (07:00 to 20:00) made during SAFS. Observations with $P(RO_X) > 0.4$ pptv s^{-1} are shown in red, and observations with $P(RO_X) < 0.2$ pptv s^{-1} are shown in blue. $P(O_3)$ for the filled points was calculated using k_{NO+HO2} as k_{eff}. This is the same as the data in Fig. 6b. Open markers show $P(O_3)$ calculated with different values for k_{eff}: $k_{NO+CH3O2}$ (squares), $k_{NO+Isoprene\ RO2}$ (stars), and $0.1*k_{NO+Acetyl\ Peroxy}+0.9*k_{NO+HO2}$ (triangles).

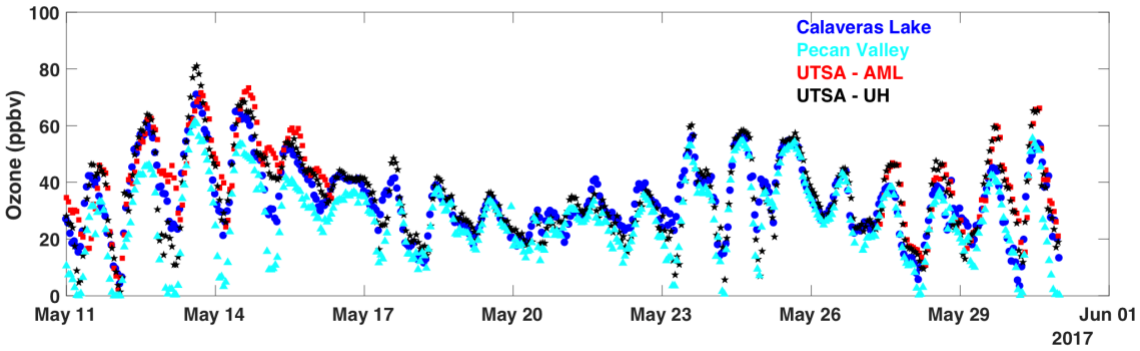

Figure S5: One-hour average O_3 at the Calaveras (blue) and Pecan Valley (cyan) TCEQ monitoring sites and at the UTSA SAFS site, including observations from both the AML (red) and by the University of Houston (black).

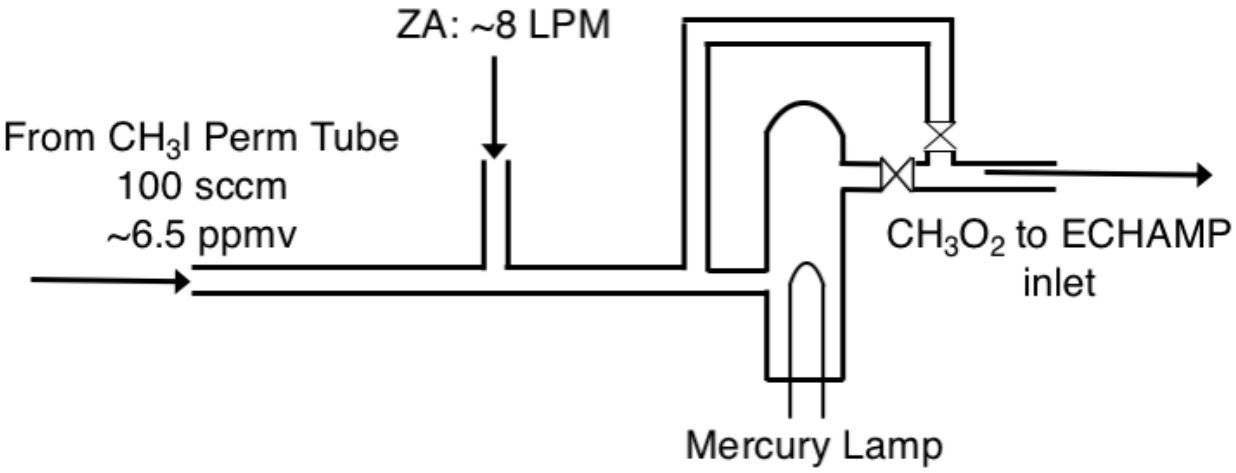

291

292 **Figure S6:** A schematic of the CH_3I calibration setup. Hourglass shapes represent two-way valves. The
293 ZA is humidified over a range of RH values from 0% to 71%.

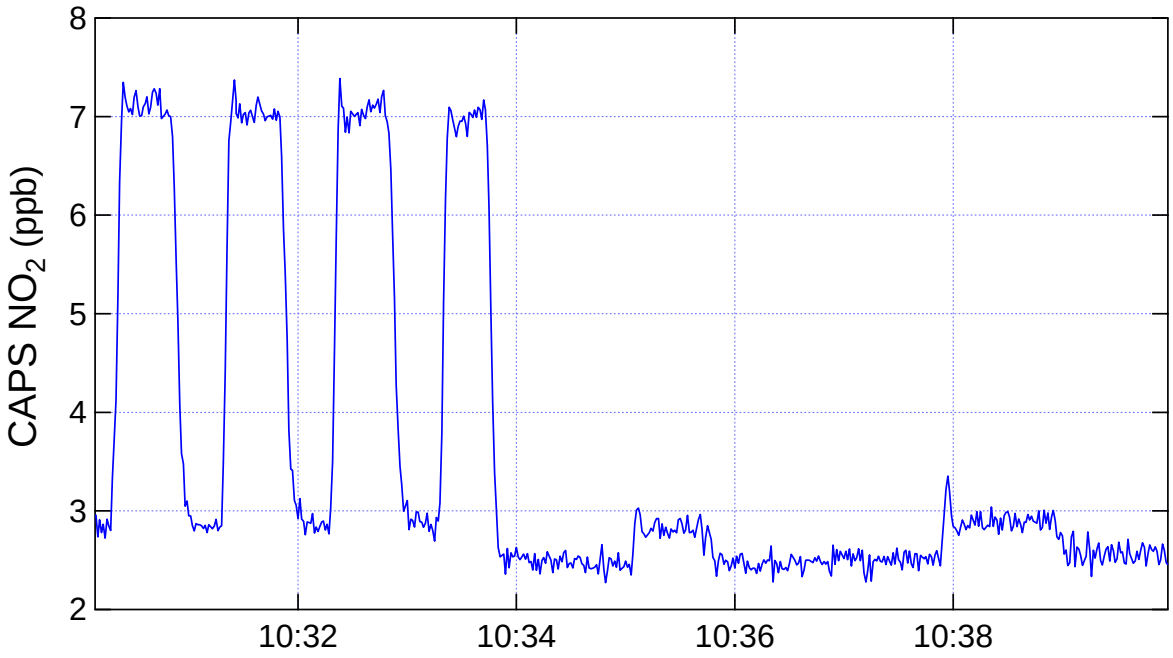

294
295 **Figure S7:** An example time series of CH_3I calibration data from 31 May 2017. From 10:30 to 10:34
296 ECHAMP operated in regular amplification mode. From 10:34 to 10:40 ECHAMP was in background
297 mode (no amplification) and the CH_3O_2 source was modulated on and off.

298

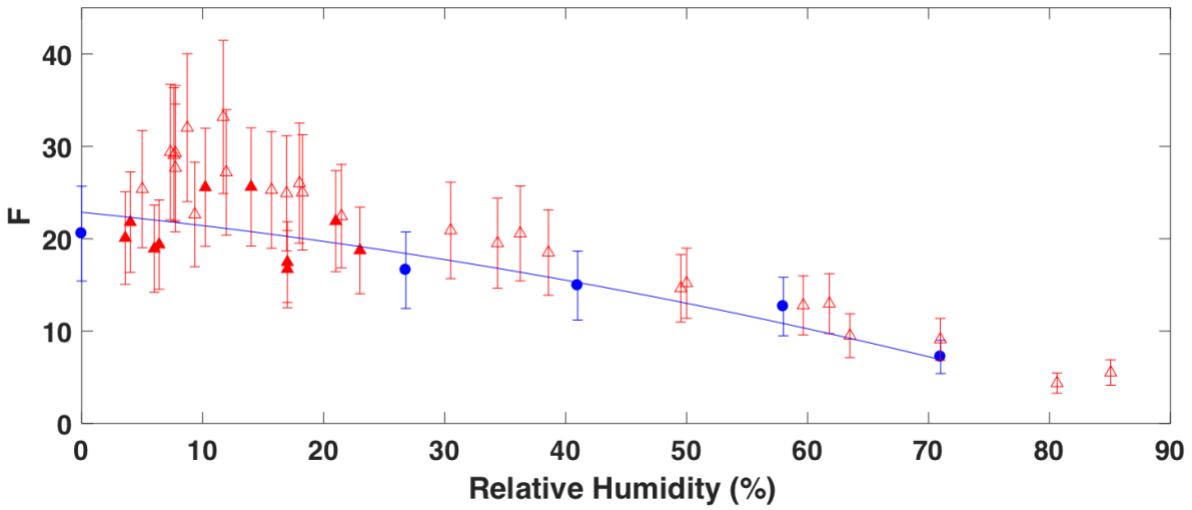

Figure S8: Calibration curve for ECHAMP during SAFS. The results from the CH_3I (blue circles) H_2O photolysis (red, filled triangles) are both shown. In addition, results from an H_2O photolysis calibration conducted during a subsequent field deployment are also shown (red, open triangles). Indicated uncertainties are the ECHAMP measurement uncertainty of 25% (2σ).

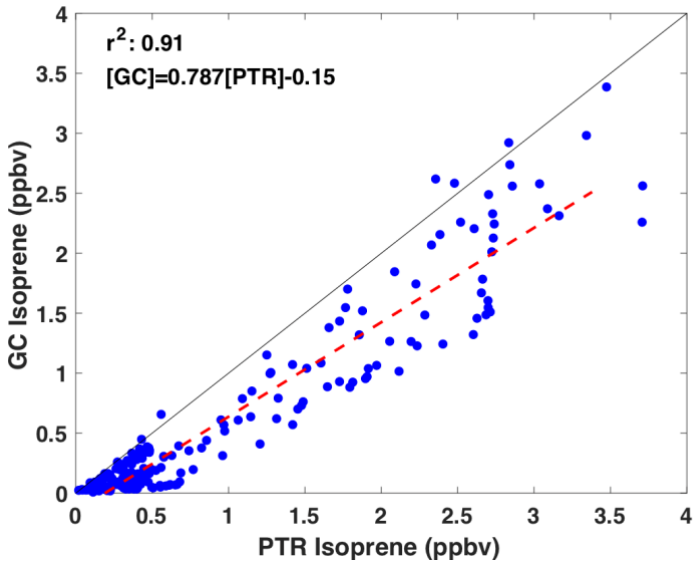

Figure S9: Comparison of isoprene measured by the PTR to observations from the GC. The isoprene sensitivity of the GC was determined several months after the campaign as described in the text.

Table S1: Description of the different simulations used to calculate the variation in INO, I_2, and CH_3O_2I with time in the CH_3I calibration setup. $k_{CH3O2+I+M}$ is the rate constant for the forward reaction of reaction S12.

	Simulation 1	**Simulation 2**	**Simulation 3**	**Simulation 4**
$[I]_0 = [CH_3O_2]_0$ (pptv)	100	1000	100	1000
$k_{CH3O2+I+M}$ (molecules cm^{-3} s^{-1})	1.0×10^{-11}	1.0×10^{-11}	1.0×10^{-10}	1.0×10^{-10}

Table S2: Rate constants at 298 K and sources for the iodine simulations. The reaction rate for Reaction S12 forward was varied as described in the text and Table S1.

Reaction	k_i (cm^3 $molecules^{-1}$ s^{-1})	Source
$I + I \rightarrow I_2$ (Reaction RS9)	3.92×10^{-13}	Jenkin et al. (1990)
$I + NO + M \rightarrow INO + M$ (Reaction RS10)	1.7×10^{-11}	Atkinson et al. (2007)
$INO + INO \rightarrow I_2 + 2NO$ (Reaction RS11)	1.3×10^{-14}	Atkinson et al. (2007)
$CH_3O_2 + I + M \rightarrow CH_3O_2I + M$ (Reaction RS12 forward)	1.0×10^{-11}	Estimate
$CH_3O_2I + M \rightarrow CH_3O_2 + I + M$ (Reaction RS12 reverse)	0	Estimate
$CH_3O_2I + I \rightarrow I_2 + CH_3O_2$ (Reaction RS13)	1.0×10^{-11}	Estimate
$CH_3O_2 + NO \rightarrow NO_2 + CH_3O$	7.7×10^{-12}	Sanders et al. (2011)

S5. References

Anderson, D.C, Pavelec, J., Lindsay, A., Wood, E.C.: Wall Loss Rates and the Use of Nafion Tubing for Selective Measurement of Peroxy Radicals. In preparation.

Atkinson, R., Baulch, D. L., Cox, R. A., Crowley, J. N., Hampson, R. F., Hynes, R. G., Jenkin, M. E., Rossi, M. J., Troe, J., and Subcommittee, I.: Evaluated kinetic and photochemical data for atmospheric chemistry: Volume II; gas phase reactions of organic species, Atmos. Chem. Phys., 6, 3625-4055, 10.5194/acp-6-3625-2006, 2006.

Atkinson, R., Baulch, D. L., Cox, R. A., Crowley, J. N., Hampson, R. F., Hynes, R. G., Jenkin, M. E., Rossi, M. J., and Troe, J.: Evaluated kinetic and photochemical data for atmospheric chemistry: Volume III - gas phase reactions of inorganic halogens, Atmospheric Chemistry and Physics, 7, 981-1191, 10.5194/acp-7-981-2007, 2007.

Cantrell, C. A., Zimmer, A., and Tyndall, G. S.: Absorption cross sections for water vapor from 183 to 193 nm, Geophysical Research Letters, 24, 2195-2198, 10.1029/97gl02100, 1997.

Clemitshaw, K. C., Carpenter, L. J., Penkett, S. A., and Jenkin, M. E.: A calibrated peroxy radical chemical amplifier for ground-based tropospheric measurements, J. Geophys. Res., 102, 25405, 10.1029/97jd01902, 1997.

Creasey, D. J., Heard, D. E., and Lee, J. D.: Absorption cross-section measurements of water vapour and oxygen at 185 nm. Implications for the calibration of field instruments to measure OH, HO_2 and RO_2 radicals, Geophysical Research Letters, 27, 1651-1654, 10.1029/1999gl011014, 2000.

Jenkin, M. E., Cox, R. A., Mellouki, A., Lebras, G., and Poulet, G.: Kinetics of the Reaction of Iodine Atoms with HO_2 Radicals, Journal of Physical Chemistry, 94, 2927-2934, 10.1021/j100370a036, 1990.

Jenkin, M. E., Saunders, S. M., Wagner, V., and Pilling, M. J.: Protocol for the development of the Master Chemical Mechanism, MCM v3 (Part B): tropospheric degradation of aromatic volatile organic compounds, Atmospheric Chemistry and Physics, 3, 181-193, 2003.

Jenkin, M. E., Young, J. C., and Rickard, A. R.: The MCM v3.3.1 degradation scheme for isoprene, Atmospheric Chemistry and Physics, 15, 11433-11459, 10.5194/acp-15-11433-2015, 2015.

Lanzendorf, E. J., Hanisco, T. F., Donahue, N. M., and Wennberg, P. O.: The measurement of tropospheric OH radicals by laser-induced fluorescence spectroscopy during the POPCORN field campaign and Inntercomparison of tropospheric OH radical measurements by multiple folded long-path laser absorption and laser induced fluorescence - Comment, Geophysical Research Letters, 24, 3037-3038, 10.1029/97gl02899, 1997.

Sanders, S. P., Friedl, R. R., Abbatt, J. P. D., Barker, J. R., Burkholder, J. B., Golden, D. M., Kolb, C. E., Kurylo, M. J., Moortgat, G. K., Wine, P. H., R.E., H., and Orkin, V. L.: Chemical Kinetics and Photochemical Data for Use in Atmopsheric Studies, 2011.

Saunders, S. M., Jenkin, M. E., Derwent, R. G., and Pilling, M. J.: Protocol for the development of the Master Chemical Mechanism, MCM v3 (Part A): tropospheric degradation of non-aromatic volatile organic compounds, Atmospheric Chemistry and Physics, 3, 161-180, 2003.

Schultz, M., Heitlinger, M., Mihelcic, D., and Volzthomas, A.: Calibration Source for Peroxy-Radicals with Built-in Actinometry using H_2O and O_2 photolysis at 185 nm, Journal of Geophysical Research-Atmospheres, 100, 18811-18816, 10.1029/95jd01642, 1995.

Wolfe, G. M., Marvin, M. R., Roberts, S. J., Travis, K. R., and Liao, J.: The Framework for 0-D Atmospheric Modeling (F0AM) v3.1, Geosci. Model Dev., 9, 3309-3319, 10.5194/gmd-9-3309-2016, 2016.

Wood, E. C., and Charest, J. R.: Chemical Amplification - Cavity Attenuated Phase Shift Spectroscopy Measurements of Atmospheric Peroxy Radicals, Analytical Chemistry, 86, 10266-10273, 10.1021/ac502451m, 2014.

Wood, E. C., Deming, B. L., and Kundu, S.: Ethane-Based Chemical Amplification Measurement Technique for Atmospheric Peroxy Radicals, Environmental Science & Technology Letters, 4, 15-19, 10.1021/acs.estlett.6b00438, 2017.